MIT Open Access Articles

EWS/FLI Confers Tumor Cell Synthetic Lethality to CDK12 Inhibition in Ewing Sarcoma

EWS/FLI confers tumor cell synthetic lethality to CDK12 inhibition in Ewing sarcoma

Amanda Balboni Iniguez[1,2], **Björn Stolte**[1,3], **Emily Jue Wang**[1,2], **Amy Saur Conway**[1], **Gabriela Alexe**[1,2,4], **Neekesh V. Dharia**[1,2], **Nicholas Kwiatkowski**[5,6,7], **Tinghu Zhang**[6,7], **Brian J. Abraham**[5], **Jaume Mora**[8], **Peter Kalev**[9], **Alan Leggett**[6,7], **Dipanjan Chowdhury**[9], **Cyril H. Benes**[10], **Richard A. Young**[5,11], **Nathanael S. Gray**[6,7], and **Kimberly Stegmaier**[1,2,*]

[1]Department of Pediatric Oncology, Dana-Farber Cancer Institute and Boston Children's Hospital, Harvard Medical School, Boston, MA 02215, USA

[2]The Broad Institute of MIT and Harvard, Cambridge, MA 02142, USA

[3]Ludwig Maximilians University of Munich, Munich 80539, Germany

[4]Bioinformatics Graduate Program, Boston University, Boston, MA 02215, USA

[5]The Whitehead Institute for Biomedical Research Cambridge, MA 02142, USA

[6]Department of Cancer Biology, Dana-Farber Cancer Institute, Boston, MA 02215, USA

[7]Department of Biological Chemistry and Molecular Pharmacology, Harvard Medical School, Boston, MA 02115, USA

[8]Development Tumor Biology Laboratory and Department of Pediatric Oncology and Hematology. Hospital Sant Joan de Déu Barcelona, 08950, Spain

[9]Department of Radiation Oncology, Dana-Farber Cancer Institute, Harvard Medical School, Boston, MA, 02215 USA

[10]Massachusetts General Hospital, Center for Cancer Research, Boston, MA 02114, USA

[11]Department of Biology, Massachusetts Institute of Technology, Cambridge, MA 02139, USA

SUMMARY

*Lead Contact to whom correspondence may be addressed: Department of Pediatric Oncology, Dana-Farber Cancer Institute, 450 Brookline Ave., Boston, MA 02215. Tel.: 617-632-4438; Fax: 617-632-4850; kimberly_stegmaier@dfci.harvard.edu.

Many cancer types are driven by oncogenic transcription factors that have been difficult to drug. Transcriptional inhibitors, however, may offer inroads into targeting these cancers. Through chemical genomics screening, we identified that Ewing sarcoma is a disease with preferential sensitivity to THZ1, a covalent small molecule CDK7/12/13 inhibitor. The selective CDK12/13 inhibitor, THZ531, impairs DNA damage repair in an EWS/FLI dependent manner, supporting a synthetic lethal relationship between response to THZ1/THZ531 and EWS/FLI expression. The combination of these molecules with PARP inhibitors showed striking synergy in cell viability and DNA damage assays *in vitro* and in multiple models of Ewing sarcoma, including a PDX, *in vivo* without hematopoietic toxicity.

IN BRIEF/eTOC
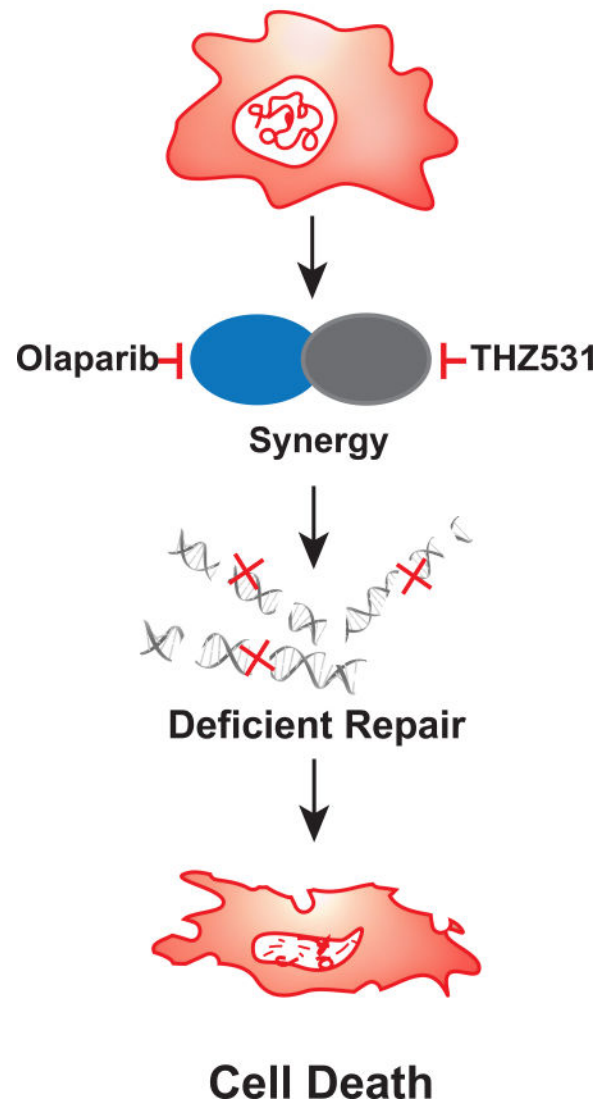
Iniguez et al. find that inhibition of CDK12 is synthetic lethal with EWS/FLI expression. CDK12/13 inhibitors impair DNA damage repair in cells expressing EWS/FLI, and the combination of CDK12/13 and PARP inhibitors synergistically reduces tumor growth and extends survival in Ewing sarcoma mouse models.

INTRODUCTION

A therapeutic challenge in oncology is the paucity of readily "druggable" genetic events in many malignancies, particularly childhood cancers. These tumors are frequently defined by sentinel abnormalities involving transcription factors in an otherwise quiet genomic landscape. Ewing sarcoma, the second most common cancer involving bone in children, is characterized by a chromosomal rearrangement that fuses the strong transactivation domain of the RNA binding protein, EWS, with the DNA binding domain of an ETS protein, most commonly FLI1. EWS/FLI acts as both a transcriptional activator and a transcriptional repressor via distinct chromatin binding mechanisms (Riggi et al., 2014), and numerous studies have demonstrated a strict dependency on EWS/FLI in Ewing sarcoma cells, supporting the targeting of this fusion protein or its transcriptional output (Hu-Lieskovan et al., 2005; Smith et al., 2006). Moreover, three recent massively parallel sequencing efforts revealed that Ewing sarcoma tumors possess very low mutation rates, harboring few recurrent mutations other than EWS/ETS rearrangements (Brohl et al., 2014; Crompton et al., 2014; Tirode et al., 2014).

One approach to treating these tumors is the direct targeting of the aberrant transcription factor. With a few notable exceptions, however, this approach poses a significant drug discovery challenge. A second approach might target a synthetic lethal dependency imparted on the cell by virtue of the cancer-promoting genetic event, such as the use of PARP inhibitors in *BRCA1*- and *BRCA2*-mutant cancers (Sonnenblick et al., 2015). A third approach might target basic transcriptional machinery with transcriptional inhibitors, such as the FDA-approved drug actinomycin D, or compounds such as THZ1, a small-molecule covalent inhibitor of CDK7/12/13.

Initial studies demonstrated that CDK7/12/13 inhibition with THZ1 may be therapeutically beneficial in tumor types that are highly dependent on transcriptional programs for initiating a transformed phenotype (Kwiatkowski et al., 2014). These studies provided rationale for an inroad into treating cancers defined by aberrant transcription factors. For example, *MYCN*-amplified neuroblastoma cells were found to be highly responsive to THZ1 through suppression of the MYCN transcriptional program, and T cell acute lymphoblastic leukemia cells (T-ALL) were responsive to THZ1 through the repression of RUNX1 (Chipumuro et al., 2014; Kwiatkowski et al., 2014). THZ1 decreases the phosphorylation of the C-terminal domain (CTD) of RNA Polymerase II (RNA Pol II), thereby preventing transcriptional initiation and elongation. Exquisite specificity is obtained through binding of the molecule to a cysteine residue adjacent to the ATP binding domain (Kwiatkowski et al., 2014). The capacity to perform at scale chemical genomic screening across over one-thousand cancer cell lines provided an unprecedented opportunity to discover new connections between response to THZ1 and the expression of other so-called "undruggable" targets.

RESULTS

Ewing sarcoma is highly sensitive to the CDK7/12/13 inhibitor THZ1

THZ1, a covalent and potent inhibitor of CDK7/12/13 kinases involved in transcriptional regulation, recently emerged as a targeted strategy to impair aberrant transcription (Chipumuro et al., 2014; Christensen et al., 2014; Kwiatkowski et al., 2014). In order to identify biomarkers of sensitivity to THZ1, we screened THZ1 against a diverse panel of 1,081 cancer cell lines (Figure 1A) (Garnett et al., 2012; Kwiatkowski et al., 2014). Within the group of cell lines highly sensitive to low concentrations of THZ1 (defined by cell lines with viability <50% when treated with 9.76 nM THZ1), Ewing sarcoma cells were significantly enriched for response (Fisher's test, $p=9\times10^{-9}$). In fact, Ewing sarcoma cell lines were collectively more sensitive to THZ1 than other cancer types previously reported to be highly sensitive to this molecule (Figure 1A). The mean viability for each tumor type screened with 9.76 nM THZ1 was as follows: Ewing sarcoma 47%, T-ALL 58%, lung cancer 92%, and neuroblastoma 96%. To assay the on-target activity of THZ1, we measured the phosphorylation of global pSer2/5/7 RNA Pol II levels at concentrations that inhibit Ewing sarcoma cell growth. THZ1 suppressed the phosphorylation of the CTD of RNA Pol II in a concentration-dependent manner (Figure 1B). Suppression of EWS/FLI did not affect the ability of THZ1 to repress these phosphorylation sites (Figure S1A). Furthermore, THZ1 induced apoptosis as demonstrated by an increase in the percentage of Annexin V$^+$ cells and PARP cleavage (Figure 1C, D) and strongly decreased the colony formation capacity of Ewing sarcoma cell lines (Figure 1E).

To establish the activity of THZ1 *in vivo*, TC32 Ewing sarcoma xenografts were treated with either vehicle control or 10 mg/kg of THZ1 delivered intraperitoneally twice per day. Treatment was stopped at day 42 and the remaining mice were followed for survival. THZ1 as a single agent significantly impaired tumor progression and increased overall survival (median survival = 28.5 days for vehicle and 44 days for the THZ1 arms) (Figure 1F, G). No weight loss-related toxicity was observed (Figure S1B).

A Primary Target of THZ1 Is CDK12 in Ewing Sarcoma

In order to elucidate preferential dependencies of cancer cells on CDK7, CDK12 and CDK13, we used genome-scale CRISPR-Cas9 screening across 341 cancer cell lines representing diverse cancer cell types (Meyers et al., 2017). We identified that *CDK7* disruption is pan-lethal with the depletion of guides targeting *CDK7* similar to the depletion seen for known common essential genes in the screen, raising some concerns about the therapeutic window of a potent CDK7 inhibitor (Figure S2A). In contrast, CDK12 and CDK13 showed differential dependencies across the cell lines included in the screen (Figure S2B, C). We found that approximately 10.2% of the cell lines are dependent on CDK12 with a dependency score of <−0.5, as compared to CDK7 and CDK13 where 100% and 3.8% of lines screened were dependent on the gene respectively. Among the CDK12 dependent cell lines was SK-N-MC, the one Ewing sarcoma cell line included in the screen harboring an EWS/FLI rearrangement, with three of the 11 neuroblastoma cell lines included in the screen scoring between −0.4 and −0.5. The majority of neuroblastoma cell lines, as well as SCLC and T-ALL cell lines, were not dependent on CDK12 for survival (Figure S2B).

Furthermore, none of the Ewing sarcoma, neuroblastoma, T-ALL or SCLC cell lines screened were dependent on CDK13 (Figure S2C). A full list of all of the CERES dependency gene scores for CDK7, CDK12, and CDK13 across the 341 cancer cell lines is included in Table S1. These data suggest that the preferential sensitivity of Ewing sarcoma cells to THZ1 in our chemical genomics screen may be due to CDK12 and not CDK7 or CDK13 inhibition. They also suggest that a more selective CDK12/13 inhibitor would be preferentially toxic to Ewing sarcoma cells and may reduce potential toxicities associated with CDK7 inhibition. In order to develop more selective molecules, Zhang et al. used THZ1 as starting material for THZ531, a first-in-class covalent and selective CDK12 and CDK13 inhibitor, which targets a cysteine residue adjacent to the ATP binding site of CDK12 and CDK13 (Zhang et al., 2016). The authors reported that THZ531 inhibits CDK12 and CDK13 with IC_{50} concentrations of 158 nM and 69 nM, respectively, whereas, THZ531 inhibits CDK7 and CDK9 at 8.5 μM and 10.5 μM, respectively (Zhang et al., 2016). Furthermore, Kinativ profiling demonstrated that CDK12 and CDK13 were the primary targets of THZ531, with none of the other 211 kinases profiled demonstrating >55% inhibition (Zhang et al., 2016). In order to identify which kinase target of THZ1 is primarily responsible for the potent anti-viability effects observed, we treated a panel of Ewing sarcoma cell lines with three compounds: THZ1, a pan CDK7/12/13 inhibitor; THZ531, a CDK12/13 selective inhibitor; and THZ531R, a non-cysteine reactive analog with reduced anti-CDK12/13 activity (Figure 2A). We found that Ewing sarcoma cell lines were nearly as sensitive to THZ531 as they were to THZ1, with IC_{50} concentrations in the low nanomolar range with both small molecules in viability assays (Figure 2A and Table S2). The mean IC_{50} for THZ1 across Ewing sarcoma cell lines was 41.03 nM vs. 90.4 nM for THZ531, demonstrating that CDK12/13 inhibition recapitulates much of the sensitivity to THZ1, although CDK7 inhibition may still contribute to the sensitivity to this molecule. Additionally, Ewing sarcoma cell lines were completely insensitive to THZ531R (Figure 2A). Furthermore, Ewing sarcoma cell lines were 3–10-fold more sensitive to THZ1 and THZ531 than non-EWS/FLI expressing osteosarcoma cell lines (Figure 2A and Table S2), suggesting that sensitivity to CDK7/12/13 inhibition may be enhanced in EWS/FLI rearranged cells. Interestingly, all ten Ewing sarcoma cell lines tested were uniformly sensitive to THZ1 and THZ531, indicating that CDK12/13 inhibition may be broadly effective as a treatment strategy for Ewing tumors defined by EWS/FLI rearrangements (Table S2).

To confirm the selectivity of these compounds in Ewing sarcoma cells, we performed THZ1-biotin immunoprecipitation of samples treated with THZ1 or THZ531 and probed for Cyclin K (binding partner of CDK12/13) or Cyclin H (binding partner of CDK7). We found that THZ531 has specificity for Cyclin K-CDK12/13 complexes and not Cyclin H-CDK7 complexes as THZ1-biotin can pull down Cyclin H-CDK7 complexes in samples pretreated with THZ531, but cannot pull down Cyclin K-CDK12/13 complexes as they are occupied by THZ531 (Figure 2B, C).

To provide further validation of the target of THZ531 in Ewing sarcoma cells, Cyclin K was knocked down in A673 Ewing sarcoma cells (Figure 2D). Suppression of Cyclin K using three different hairpins strongly suppressed the viability of these cells (Figure 2D, E). To further discriminate which CDK is responsible for the potent growth suppression with

THZ531, we knocked down CDK12 and CDK13 using two different hairpins (Figure 2F). We found that genetic suppression of CDK12 decreased the viability of Ewing sarcoma cells (Figure 2F, G), while in contrast, suppression of CDK13 had a minimal effect (Figure 2F, G). Additionally, CRISPR-Cas9 mediated knockout of *CDK12* strongly reduced Ewing sarcoma cell viability (Figure 2H, I). Collectively, these results demonstrate that CDK12 inhibition underlies the enhanced sensitivity of Ewing sarcoma cells to THZ1, and as such, we focused on the more selective compound, THZ531.

Cyclin K/CDK12 and Cyclin K/CDK13 complexes were recently identified in human cells (Blazek et al. 2011). The Cyclin K/CDK12 complex has been shown to regulate the phosphorylation of the CTD of RNA Pol II (Blazek et al., 2011). Consistent with the effects of THZ1, THZ531 reduced the phosphorylation of the RNA Pol II CTD at Ser2 and Ser5, but in contrast, did not strongly reduce the phosphorylation at Ser7 (Figure S2D). Additionally, THZ531 increased PARP cleavage and Annexin V[+] cell populations and decreased anchorage independent growth in soft agar in Ewing sarcoma cells (Figure S2E–G).

THZ531 Treatment Preferentially Represses the Expression of DNA Repair-related Genes in Ewing Sarcoma Cells

We next performed global gene expression profiling to investigate the effects of THZ531 on transcriptional programs in Ewing sarcoma. We profiled two highly sensitive EWS/FLI rearranged Ewing sarcoma cell lines, A673 and TC32, for which we have deep genomic characterization (Crompton et al., 2014). Samples were treated in duplicate with DMSO or THZ531 at 100 nM or 500 nM for 6 hr. THZ531 treatment globally downregulated steady-state mRNA levels in a concentration-dependent manner (Figure 3A). We observed profound gene expression suppression at 500 nM in both cell lines with 22% and 27% of genes downregulated >2 linear fold in A673 and TC32 cells respectively (4,159 out of 18,712 genes in A673 cells and 4,207 out of 15,546 genes in TC32 cells) (Figure 3A). More modest effects on gene expression were observed at the 100 nM concentration with 10% and 6.7% of genes downregulated > 2-fold in A673 and TC32 cells respectively (1,876 out of 18,712 genes in A673 cells and 1,142 out of 15,546 genes in TC32 cells) (Figure 3A). Remarkably few genes were upregulated by THZ531 at either 100 nM or 500 nM, consistent with the known role of CDK12/13 in transcriptional initiation and elongation. The numbers of differentially expressed genes observed with THZ531 treatment is consistent with the differential expression observed with genetic depletion of *CDK12* (Liang et al., 2015). Gene expression changes between A673 and TC32 cells were strongly correlated at both 100 nM (R^2=0.67) and 500 nM ($R^2 = 0.72$) of THZ531 (Figure 3B). Venn diagrams demonstrate the significant overlap of downregulated and upregulated genes between the two cell lines (Figure S3A, B), indicating a common gene expression response to THZ531.

To elucidate candidate mechanisms of action of THZ531 in Ewing sarcoma, genes were ranked from most to least sensitive to 100 nM THZ531, and the top 5% of THZ531-sensitive genes (944 genes for A673 and 788 genes for TC32) were subjected to gene ontology enrichment using David functional annotation software analysis (Figure 3C). As expected, gene sets related to regulation of transcription and replication were enriched among

THZ531–responsive genes. Additionally, genes involved in DNA damage repair were identified as being preferentially downregulated by THZ531. We then performed Gene Set Enrichment Analysis (GSEA) for enrichment in the 5,499 gene sets from the MSigDB v5 collections, c2 (curated pathways and experimental gene sets) and c5 (Gene Ontology), as well as published EWS/FLI genes sets (Figure 3D) (Marques Howarth et al., 2014; Tomazou et al., 2015). Several DNA damage response (DDR) gene sets fell above the threshold of statistical significance and had negative normalized enrichment scores (NES) (Figure 3D), indicating that these gene sets were significantly downregulated by THZ531 treatment in both A673 and TC32 cells. DNA damage checkpoint and homologous recombination gene sets were among the most depleted by THZ531 treatment (Figure 3E). Furthermore, there was a noticeable lack of significant downregulation of EWS/FLI gene sets by THZ531 treatment in both Ewing sarcoma cell lines (Figure 3D). Lists of all DDR and EWS/FLI gene sets are included in Tables S3 and S4 and of all genes affected by THZ531 treatment in Table S5.

Several key genes regulating DDR were downregulated by THZ531 in A673 and TC32 cells (Figure 3F). We performed a leading edge analysis to identify the genes that form the consensus among the DNA damage and repair gene signatures. We found that 33 genes belong to at least four of the enriched DNA damage and repair MSigDB gene sets, including several genes regulating homologous recombination and UV response (Figure S3C). Low-throughput validation of select genes (*BRCA1*, *RAD51*, *FANCF*, *XRCC2*) by qPCR confirmed that THZ531 strongly suppresses expression of these genes (Figure S3D).

As THZ1 has been reported to preferentially repress the expression of super-enhancer (SE)-marked genes, we analyzed the effect of THZ531 on SE-marked gene expression (Chipumuro et al., 2014; Christensen et al., 2014; Kwiatkowski et al., 2014). Box plots show the log-fold change (LFC) in gene expression of all genes, typical enhancer-associated genes (TE), SE genes, and EWS/FLI target genes following THZ531 treatment (Figure S3E). In this analysis, enhancers were ranked by H3K27Ac ChIP-sequencing signal, and EWS/FLI target genes were identified as 1) genes associated with EWS/FLI ChIP-sequencing signal and 2) genes with a decrease in transcript expression following EWS/FLI knockdown in A673 cells as described in Riggi et al. 2014 (Riggi et al., 2014). Interestingly, we found that SE-associated genes and EWS/FLI target genes were not preferentially repressed by THZ531 compared to all genes. This data suggests that CDK12 and CDK13 do not preferentially regulate SE-marked or EWS/FLI target genes in Ewing sarcoma.

EWS/FLI Expression Imparts Sensitivity to CDK12 Inhibition and to Molecules Inducing DNA Damage

In light of the exceptional sensitivity of Ewing sarcoma cells to THZ531, we hypothesized that EWS/FLI may render cells more vulnerable to THZ531 and other DNA damage repair inhibitors. Indeed, DNA damaging agents are currently used to treat patients with Ewing sarcoma, and Ewing sarcoma cell lines have been reported to be highly sensitive to PARP inhibitors (Gill et al., 2015). To test this hypothesis, we knocked down EWS/FLI using a TRIPZ inducible system. We found that EWS/FLI suppression using two unique hairpins rendered TC32 and A673 cells less sensitive to THZ531 (Figure 3G, H). Furthermore,

suppression of EWS/FLI can partially rescue the anti-viability effects of CDK12 knockdown (Figure 3I). To rule out the possibility that EWS/FLI knockdown renders resistance to THZ531 due to induction of cell cycle arrest, we serum starved A673 and TC32 Ewing sarcoma cells to induce growth-arrest (Figure S3F, G) and assayed sensitivity of these cells to THZ531. Importantly, unlike cells with EWS/FLI suppression, serum starved cells do not display differential sensitivity to THZ531 (Figure S3H, I). Thus, the proliferative disadvantage of losing EWS/FLI is not responsible for the increased resistance to THZ531 as inducing growth-arrest with serum starvation does not engender resistance to these molecules. These results suggest that the EWS/FLI oncoprotein imparts vulnerability to compounds that induce defects in DNA damage repair and suggest that the presence of EWS/FLI itself is synthetic lethal with CDK12 inhibition in Ewing sarcoma cells.

We next mined the Genomics of Drug Sensitivity in Cancer (GDSC) database, a screen of 1,074 cancer cell lines treated with 265 anti-cancer drugs, to identify additional small molecules for which EWS/FLI is a biomarker of response (Yang et al., 2013). There was significant enrichment for drugs inducing DNA damage among the compounds in which EWS/FLI rearrangement was a biomarker of sensitivity (Figure 3J). Among these compounds were mitomycin-C, etoposide, SN-38, camptothecin, and gemcitabine, all of which are chemotherapeutic agents that induce DNA damage. EWS/FLI was also a biomarker of sensitivity to the ATM inhibitor, CP466722, an interesting finding in light of a recent publication identifying ATR inhibitors as active in Ewing sarcoma (Nieto-Soler et al., 2016). Additionally, as previously reported, EWS/FLI was a biomarker of sensitivity to three different PARP inhibitors (Figure 3J) (Garnett et al., 2012).

THZ531 Is Synergistic with PARP Inhibitors in Ewing Sarcoma

While THZ1 was active in a mouse model of Ewing sarcoma, treatment with THZ1 as a single agent did not cure mice of disease, suggesting that combination therapy will be necessary to achieve full efficacy. Therefore, we sought to identify clinically tractable synergistic combinations with THZ1 in Ewing sarcoma models. Ovarian tumors with loss-of-function mutations in *CDK12* have reduced BRCA1 levels, deficient HR, and are highly sensitive to PARP inhibition (Joshi et al., 2014). Moreover, it was recently reported that pan-CDK inhibition with dinaciclib can reverse PARP inhibitor resistance in BRCA-mutated triple negative breast cancer (Johnson et al., 2016). In Ewing sarcoma, studies have demonstrated that EWS/FLI physically interacts with PARP1, and induces PARP1 expression (Brenner et al., 2012; Garnett et al., 2012; Stewart et al., 2014; Yang et al., 2013). These previous studies, in addition to our gene expression data identifying that THZ531 preferentially downregulates HR repair genes in Ewing sarcoma, led us to hypothesize that THZ531 would synergize with PARP inhibitors. We used the Bliss independence and Loewe additivity models to assess synergy. The Bliss independence model computes a quantitative measure, excess over Bliss (eob), the difference between the observed combined effect and the expected combined effect of the two drugs (Bliss, 1956; Greco et al., 1995), while the Chou-Talalay Combination Index (CI) for the Loewe additivity model is a dose-effect approach that estimates the effect of combining two drugs based on the dose of each individual drug that produces the same quantitative effect (Chou, 2006; Chou and Talalay, 1984). We observed strong synergy between THZ531 and olaparib in several Ewing sarcoma

cell lines using both models across a wide range of concentrations (Figure 4A, B). Moreover, we observed that THZ531 strongly synergizes with cisplatin, mitomycin C, the ATR inhibitor VE821, and the ATM inhibitor KU5593, in Ewing sarcoma cells (Figure S4A–D). Importantly, THZ531 does not synergize with vincristine, a microtubule inhibitor not classified as a DNA damaging agent (Figure S4E). This data provides further support that THZ531 mechanistically works through inhibiting DNA damage repair. Taken together, these findings suggest that Ewing sarcoma is a disease marked by DNA damage repair deficiency rendering tumor cells highly sensitive to these combination strategies.

To confirm the on-target activity of THZ531 in this combination effect, we knocked down CDK12 and CDK13, treated these cells with olaparib, and assayed for cell viability. We found that genetic suppression of CDK12, but not CDK13, sensitizes cells to olaparib (Figure 4C). This data supports that inhibition of CDK12 is responsible for the defects in DNA damage repair induced by THZ531. Furthermore, we demonstrated that suppression of EWS/FLI using two different hairpins renders cells more resistant to olaparib (Figure 4D), and when EWS/FLI is suppressed, synergy between THZ531 and olaparib is abrogated, consistent with the notion that EWS/FLI imparts vulnerability to defects in DNA repair (Figure 4E).

To further investigate the effects of these compounds on DNA damage and repair, we performed immunofluorescent analysis of γH2AX, an early sensor of DNA double strand breaks. THZ531 and olaparib alone induced γH2AX foci staining in Ewing sarcoma cells (Figure 5A, B), and the combination synergistically induced γH2AX foci formation, suggesting that this combination impairs the ability of Ewing sarcoma cells to repair DNA damage. To evaluate the effects on HR repair, we assayed RAD51 foci staining, a key regulator of HR-mediated repair. We observed a striking increase in RAD51 foci staining in Ewing sarcoma cells treated with olaparib (Figure 5C, D). Interestingly, THZ531 prevented the induction of RAD51 foci formation in olaparib-treated Ewing sarcoma cells, suggesting that THZ531 is impairing HR and the ability of RAD51 to be recruited to sites of DNA damage. We found that both THZ531 treatment and knockout of *CDK12* led to a decrease in total RAD51 protein levels (Figure 5E, F). Furthermore, we observed a decrease in cell viability when *RAD51* was knocked out by CRISPR-Cas9 (Figure 5G, H).

The Combination of CDK7/12/13 and PARP Inhibitors Is Highly Active in Ewing Sarcoma

We next assayed the *in vivo* efficacy of combining a CDK12 inhibitor and olaparib in a mouse model of Ewing sarcoma. Because THZ531 is not optimized for *in vivo* studies, we used the parental compound, THZ1. We first confirmed synergy between the parental molecule and olaparib *in vitro* (Figure S5A). We then established an A673 xenograft mouse model of Ewing sarcoma and performed a 4-arm study with twice-daily (BID) treatment of vehicle, 10 mg/kg THZ1, 50 mg/kg olaparib, and the combination of olaparib+THZ1 delivered for 40 days. Olaparib and THZ1 as single agents each significantly decreased tumor growth rate and extended the survival of the mice (median survival = 18 days vehicle, 32 days THZ1 and 28 days in the olaparib groups) (Figure 6A, B). A striking decreased tumor growth rate was observed when both drugs were used in combination (Figure 6A), and the combination treatment significantly extended survival compared to the vehicle

control or either single agent (Figure 6B). Seventy percent of mice in the combination arm were still alive by day 40 when treatment was ended (Figure 6B). Mice were followed out to day 150 without further treatment. At day 60, 40% (4 out of 10) of the mice in the combination group were still alive, whereas all of the mice in the vehicle and single agent arms had been sacrificed. Furthermore 20% of tumors in the combination arm had regressed to where they were no longer palpable (Figure 6B). In order to test the generalizability of this treatment strategy in Ewing sarcoma, we performed combination *in vivo* studies in a second xenograft mouse model using TC71 cells as well as a patient-derived xenograft (PDX) mouse model of this disease. In the TC71 xenograft study, both THZ1 and olaparib significantly reduced the tumor growth rate and extended survival as single agents (Figure 6C, D), and the combination of THZ1 and olaparib significantly reduced tumor growth rate compared to either agent used alone (Figure 6C). The median survival of mice in the vehicle treated group was 30.5 days, compared to 42 days in the olaparib group, 38.5 days in the THZ1 group and 66.5 days in the combination group (Figure 6D). Furthermore, we established a PDX mouse model of Ewing sarcoma with a type I EWS/FLI fusion from a tumor resected from the fibula of a 12 year old patient at diagnosis (HSJD-ES-002). In this model, THZ1 as a single agent did not significantly reduce the tumor progression (Figure 6E) but did significantly increase overall survival (Figure 6F). Importantly, the combination of THZ1 and olaparib strikingly reduced tumor progression and increased survival in this PDX (Figure 6E, F): vehicle, 23 days; olaparib, 42 days; THZ1, 44 days; and combination, 56 days. Taken together, this drug combination resulted in a more profound and durable response than treatment with either drug alone.

Complete blood counts of all mice treated with THZ1 and olaparib and the combination of these two drugs in the TC71 xenograft mouse model of Ewing sarcoma were performed (Figure 6G). Importantly, we did not observe any hematopoietic toxicities after up to 40 days of treatment. Significant weight loss was also not observed in any of the three mouse models tested over long-term treatment (Figure S5B–D).

DISCUSSION

Pediatric, and even a subset of adult, cancers possess remarkably quiet genomes that are defined by sentinel genetic lesions (Lawrence et al., 2013). In principle, targeting these key lesions should make for a propitious therapeutic strategy; however, because most of the driver events involve transcription factors or loss of tumor suppressors, only a minority have been successfully pharmacologically addressed. For example, chromosomal translocations that result in EWS/ETS rearrangements characterizing Ewing sarcoma tumors have yet to be successfully targeted. EWS/FLI is a master transcription factor which activates an oncogenic transcriptional program. Unfortunately, targeting this transcription factor fusion protein has been a drug discovery challenge. Here, we demonstrate that synthetic lethal dependencies can be identified in the context of sentinel genetic lesions using chemical genomics. We determined that EWS/FLI incurs a synthetic lethal relationship with molecules that are involved in DNA damage/repair. Such a strategy could be applied broadly to other cancers with exceptionally simple genomic landscapes.

DNA damaging agents, such as doxorubicin and etoposide, form the backbone of Ewing sarcoma therapy. Moreover, Ewing sarcoma is highly radiation responsive, suggesting that Ewing sarcoma is particularly sensitive to DNA damage. Intriguingly, three independent studies reported that Ewing sarcoma is sensitive to PARP inhibitors (Brenner et al., 2012; Garnett et al., 2012; Stewart et al., 2014; Yang et al., 2013). In one study, PARP1 was found to physically interact with EWS/FLI and act as a transcriptional co-regulator of the oncogenic transcription factor fusion protein (Brenner et al., 2012). Furthermore, EWS/FLI was found to induce PARP1 expression in a positive feed forward loop (Brenner et al., 2012). In a second study, a chemical genomics screen across 639 cancer cell lines was conducted to identify new genotype:chemosensitivity relationships in cancer (Garnett et al., 2012; Yang et al., 2013). The connection between EWS/ETS rearranged Ewing sarcoma and response to PARP inhibitors was highlighted. Suppressing EWS/FLI in Ewing sarcoma cells was reported to render resistance to PARP inhibition, a finding which we recapitulate in the current study (Garnett et al., 2012). In our own study of the exquisite sensitivity to the CDK7/12/13 inhibitor THZ1, we found that CDK12 was an essential target for their selective sensitivity, and mechanistically, suppression of RAD51 expression impaired the growth of EWS/FLI-expressing Ewing sarcoma cells. Our data are consistent with prior studies demonstrating that CDK12 regulates the expression of DNA damage repair genes, most notably, *BRCA1*, *ATR*, *FANCI* and *FANCD2* (Blazek et al., 2011). Furthermore, CDK12 was shown to bind to these HR-related genes and was necessary for the phosphorylation of the CTD of RNA Pol II at Ser2 at these genes (Ekumi et al., 2015).

While additional studies will be necessary to dissect the precise mechanisms by which EWS/FLI sensitizes Ewing sarcoma cells to compounds that induce DNA damage and/or prevent its repair, the results of these studies are readily translatable. Clinical trials testing PARP inhibitors in patients with BRCA-deficient tumors have demonstrated anti-tumor efficacy and provide an example of successfully exploiting synthetic lethal relationships for therapeutic benefit (Kaelin, 2005; Sonnenblick et al., 2015). The promising activity of PARP inhibitors in trials for HR deficient tumors, and the convergence of multiple groups demonstrating PARP inhibitor activity in Ewing sarcoma, prompted much interest in their clinical testing in this disease, one for which there are no approved targeted therapeutics and for which cure rates remain quite poor for patients with metastatic or relapsed disease. Despite promising preclinical data demonstrating sensitivity of Ewing sarcoma cells to PARP inhibitors (Norris et al., 2014; Vormoor and Curtin, 2014), a Phase II clinical trial testing olaparib in patients with relapsed/refractory Ewing sarcoma failed to demonstrate anti-tumor efficacy (Choy et al., 2014). These disappointing results highlighted the need to identify agents to use in combination with PARP inhibitors to improve their efficacy.

In the current study, we hypothesized that a CDK12 inhibitor would synergize with a PARP inhibitor because *CDK12* loss-of-function mutations in ovarian cancer have rendered sensitivity to PARP inhibitors (Bajrami et al., 2014; Joshi et al., 2014). Indeed, THZ531/ THZ1 and olaparib were highly synergistic *in vitro*, and THZ1 and olaparib were highly active in combination *in vivo* with a subset of the mice remarkably "cured" of disease without bone marrow toxicity. It is important to note that some of the anti-proliferative effects of THZ1 *in vivo* may not be due solely to CDK12 inhibition, as the molecule also targets CDK7 and CDK13, and the optimization of CDK12 selective inhibitors for *in vivo*

studies is still needed. However, the strong synergy observed between THZ1 and olaparib is likely mediated by THZ1's inhibitory effects on CDK12, which our data suggests impairs HR repair. With this class of compounds in early phase clinical trials, this study has translational potential for patients with Ewing sarcoma and provides the preclinical validation for second-generation clinical trials. Moreover, this combination is predicted to be broadly applicable for cancers with *BRCA1/2* mutations, which are highly sensitive to PARP inhibitors.

Contact for Reagent and Resource Sharing

Requests for resources and reagents should be directed to and will be fulfilled by the Lead Contact, Kimberly Stegmaier (kimberly_stegmaier@dfci.harvard.edu)

Experimental Model and Subject Details

Cell Lines

A673 cells (female) were cultured in DMEM + 10% FBS + 1mM sodium pyruvate + 1% PSQ. TC32 (female), TC71 (male) and SJSA1 (male) cells were cultured in RPMI + 10% FBS +1% PSQ. EW8 (male), U2OS (female), and SKNMC (female) cells were cultured in DMEM + 10% FBS + 1% PSQ. EWS502 cells (female) were cultured in DMEM + 15% FBS + 1% PSQ. RDES (male), EWS834 (female), and SKNEP1 (female) cells were cultured in DMEM + 20% FBS + 1% PSQ. SKES1 (male) cells were cultured in McCoys5a + 15% FBS + 1% PSQ. Whole exome sequencing, RNA sequencing and STR genotyping of all Ewing sarcoma cell lines used in these studies were previously performed to validate cell line identity (Crompton et al., 2014).

In Vivo Tumor Models

A PDX mouse model of Ewing sarcoma with a type I EWS/FLI fusion was established from a tumor resected from the fibula of a 12 year old patient at diagnosis (HSJD-ES-002). HSJD-ES-002 was established in athymic nude mice (Harlan, Barcelona, Spain) as previously described (Monterrubio et al., 2015; Ordonez et al., 2015). Informed consent for the use of clinical data and biological material was obtained from the patient and all studies were approved by the ethics review committee at the Sant Joan de Déu Hospital in Esplugues de Llobregat. All dosing studies were performed at the Dana-Farber Cancer Institute, and all animal protocols were approved by the Dana-Farber Cancer Institute Animal Care and Use Committee. Nude mice were maintained according to institutional guidelines.

Single agent THZ1 study—Three million TC32 Ewing sarcoma cells were implanted subcutaneously into the right flank of 7–8 week old female nude mice. Following engraftment, mice with palpable tumors were divided into two groups and treated with 10 mg/kg THZ1 or vehicle control administered IP BID. Tumors were measured twice per week and mice were followed for survival. Statistical significance was determined by Log-rank test for survival curves.

THZ1 and olaparib combination study—Three million A673 or TC71 cells were subcutaneously implanted into the right flanks of 7–8 week old nude female mice. For PDX

studies, 1 mm^3 viably frozen tumor chunks were dipped in matrigel and implanted into the right flanks via minor surgery. When tumors measured 100–150 mm^3, mice were divided into four groups: vehicle control, THZ1, olaparib, and THZ1 and olaparib in combination. THZ1 was administered IP BID at 10 mg/kg, and olaparib was administered PO BID at 50 mg/kg. Tumors were measured twice per week and mice were followed for survival. Statistical significance was determined by log-rank test for survival curves.

Method Details

Western Blotting

Cells were lysed in Cell Signaling Lysis Buffer (Cell Signaling Technology) supplemented with Complete, EDTA free Protease Inhibitor Cocktail (Roche Diagnostics) and PhosSTOP Phosphatase Inhibitor (Roche Diagnostics). Protein concentrations were determined by the Bradford protein assay. Protein samples were separated by SDS-PAGE and transferred to PVDF membranes. Membranes were incubated with primary antibodies directed against CDK7 (Cell Signaling Technology Cat. No. 2090S), CDK12 (Cell Signaling Technology Cat. No. 11973), CDK13 (Bethyl Cat. No. A301-458A), Cyclin K (Abcam ab130475), p-Ser2-RNA-Pol II (Bethyl Cat. No. A300654A), p-Ser5-RNA-Pol II (Bethyl Cat. No. A300-655A), p-Ser7-RNA-Pol II (Millipore Cat. No. 04-1570), total RNA-Pol II (Santa Cruz Cat. No. sc-17798), PARP (Cell Signaling Technology Cat. No. 9542), RAD51 (Cell Signaling Technology Cat. No. 8875), FLI1 (Santa Cruz Biotechnology Cat. No. sc-356), Vinculin (Abcam Cat. No. ab18058), GAPDH (Santa Cruz Biotechnology Cat. No. sc-137179), and β-Actin (Cell Signaling Technology Cat. No. cs3700). Horseradish peroxidase (HRP) conjugated secondary antibodies were used. Blots were visualized by enhanced chemi-luminescence (ThermoFisher Scientific).

Quantitative PCR

RNA was extracted from cells with the RNeasy Kit and on-column DNA digestion (Qiagen). cDNA was prepared using M-MLV Reverse Transcriptase (ThermoFisher Scientific). Taqman probes for *RPL13A* (Hs01926559_g1), *BRCA1* (Hs01556193_m1), *RAD51* (Hs00427442_m1), *FANCF* (Hs00256030_s1), and *XRCC2* (Hs03044154_m1) were obtained from Life Technologies. Data were collected in technical and biological triplicate and analyzed using the   CT method.

Compounds

THZ1, THZ1R, THZ531, and THZ531R were synthesized by the Gray Laboratory (Dana-Farber Cancer Institute). Olaparib was obtained from Selleck Chemicals (Cat. No. S1060) for *in vitro* studies, and ApexBio (Cat. No. A4154) for *in vivo* studies. For the *in vivo* studies, THZ1 was solubilized in 10% DMSO, 90% D5W, and olaparib was solubilized in 10% DMSO, 90% HPBCD.

THZ1-biotin immunoprecipitation

Cell were treated with THZ1 or THZ531 for 6 hr and lysed with 50 mM Hepes pH 7.4, 150 mM NaCl, 1% NP40, 5 mM EDTA, and protease and phosphatase inhibitors. Samples were incubated with 1 μM THZ1-biotin or DMSO overnight at 4°C. Streptavidin beads were

added to each sample and incubated for 2 hr at 4°C. Samples were washed in lysis buffer and SDS loading dye was added to each sample and boiled at 95°C before loading onto western blot gels.

Genome-scale CRISPR-Cas9 Screening

The genome-scale CRISPR-Cas9 screen was conducted using the Broad Institute's Avana library and analyzed using the CERES algorithm as previously described (Meyers at al., 2017). The data used for the analysis of CDK7, CDK12, and CDK13 included the gene effects as predicted by the CERES algorithm.

RNA Extractions and Synthetic RNA Spike-in

RNA was extracted from equal numbers of Ewing sarcoma cells using the RNeasy kit (Qiagen) according to the manufacturer's instructions. A fixed amount of External RNA Controls Consortium (ERCC) RNA Spike-In Mix (Ambion, 4456739) was added to the total RNA (Loven et al., 2012).

Gene Expression Profiling

Gene expression profiling was performed with spiked-in RNA samples using Human PrimeView arrays (Affymetrix) as previously described (Kwiatkowski et al., 2014). For gene expression studies, the CEL data files were subjected to the quality control tests based on distance between arrays, array intensity distribution and variance mean dependence, which are implemented in the ArrayQuality R package available at Bioconductor v 3.2 (www.bioconductor.org). All CEL files passed the test. CEL files were processed as previously described (Kwiatkowski et al., 2014). Briefly, the raw expression values for each probe were summarized using Mas5, and Mas5-normalized probe set values were normalized across samples using Loess normalization with ERCC probes as the reference subset. The probe with the highest average signal was taken for each RefSeq transcript. Replicates were averaged for each transcript. All probe sets with an average log2 expression below 4 were considered under-expressed and they were designated as "filtered". Out of the 49,293 probe sets on the Affymetrix PrimeView Human Gene Expression Array, 44,125 probe sets remained after filtering. The data from the 44,125 probe sets was further collapsed to 11,963 non-redundant genes with distinct GRCh37/hg19 HUGO symbols, by assigning to each gene the probe set with the maximum average expression intensity. These genes were considered expressed for Figure 3A and F. For each cell line, significant hits were selected based on the cutoffs: 1 for absolute fold change, 0.05 for permutation p value, and 0.05 for False Discovery Rate. Transcript fold-changes were performed by log2-transforming the transcript values in both samples plus one pseudo-count and subtracting the log2-transformed values. In Figure 3F, the top 30% of transcripts ranked by DMSO signal were taken.

Gene Set Enrichment Analysis

The Database for Annotation, Visualization and Integrated Discovery (DAVID) v6.7 and the GSEA v2.1.0 software were used to identify functional associations of the molecular phenotypes induced by THZ531 at 100 nM vs. vehicle and by THZ531 at 500 nM vs.

vehicle. Gene sets with less than 15 genes or more than 500 genes were excluded from the analysis. Gene sets with an FDR 0.25 and a nominal p value 0.05 were considered significant hits. The enrichment results for THZ531 at 100 nM vs. vehicle and for THZ531 at 500 nM vs. vehicle were visualized on GSEA plots and heatmaps for selected gene signatures. The molecular gene set signatures of THZ531 100 nM and THZ531 500 nM vs. vehicle were visualized as dots in the volcano plots of normalized enrichment scores (NES) vs. $-\log10$(p value) scores.

Comparative Marker Analysis

The Comparative Marker Selection module from GenePattern v3.9.6 was employed to identify individual genes that were differentially expressed between treated and vehicle conditions. The analysis was performed on the log2 normalized expression data by applying a 2-sided signal-to-noise ratio (SNR) test followed by 1000 permutations of phenotype labels. The settings for the SNR parameters were log-transformed-data: yes, complete:no, balanced:no, smooth p values: yes. Gene signatures (down and up) for 100 nM THZ531 vs. vehicle and 500 nM THZ531 vs. vehicle were defined separately for each of the A673 and TC32 cell lines based on the cut-offs SNR permutation p value 0.05, Benjamini-Hochberg false discovery rate (FDR) 0.05, and absolute fold change [FC] 2. A *core* molecular signature for the differential expression of A673 and TC32 cell lines was defined by overlapping the lists of genes which are significantly differentially expressed (down and up, respectively) in either cell line. The significance of the overlap of the lists of genes differentially expressed in A763 vs. TC32 cell lines was estimated based on the two-tailed Fisher test. The correlation between the expression fold changes induced by THZ531 vs. vehicle in the A673 and TC32 cell lines was estimated by fitting a linear regression model. The differentially expressed genes induced by THZ531 in the A673 and TC32 cell lines were visualized as highlighted dots in scatter plots of log2 fold change of expression.

Super-Enhancer Analysis

The TC32 enhancer and FLI1 region/gene target data were created and published by the Stegmaier lab (Kennedy et al., 2015). The A673 enhancer and FLI1 region/gene target data were created and published by the Rivera lab (Riggi et al., 2014). Peaks were called using MACS 1.4.2 with corresponding input control and two parameter sets:-p 1e-9 --keep-dup=1 and -p 1e-9 --keep-dup=all. The collapsed union of peaks was used as input for ROSE. ROSE was run with parameters -t 1000 -s 12500 and corresponding input control. ROSE-defined enhancers were assigned to the single nearest expressed gene whose transcription start site was closest to the center of the enhancer. Expressed genes are defined as the top 2/3 of RefSeq transcripts ranked by their promoter H3K27ac levels, where promoters are defined as 1kb regions centered on each transcription start site and H3K27ac level is calculated using bamToGFF (https://github.com/BradnerLab/pipeline) with parameters -e 200 -m 1 -r -d.

Leading Edge Analysis The leading edge analysis implemented in the GSEA platform http://software.broadinstitute.org/gsea/index.jsp was employed to analyze the collection of "leading edge" genes, (i.e., the genes which simultaneously (i) are in multiple significantly enriched DNA Damage and DNA Repair gene sets and (ii) are differentially expressed by

the THZ531 100 nM treatment vs. vehicle). The collection of 33 leading edge genes that belong to at least four DNA Damage and DNA Repair gene sets enriched in the THZ531 vs. vehicle signature was visualized.

Immunofluorescence

Cells were fixed with 4% paraformaldehyde for 10 minutes at RT, permeabilized with ice cold methanol for 5 minutes at −20°C, and blocked in 3% BSA in PBS for 30 minutes at RT. Cells were then incubated in primary antibodies against RAD51 (Abcam, clone 14B4), or γH2AX (S139, Millipore, clone JBW301). Alexa-Fluor conjugated secondary antibodies were used (Life Technologies). Cell nuclei were stained using DAPI reagent (Cell Signaling Technology Cat. No. 8961). One hundred cells per sample were counted. A cell was counted as γH2AX or RAD51 positive only if >10 foci per nucleus were identified.

Colony Formation Assays

A base layer of 1:9 6% agar in media was poured into 24 well plates. Cells were plated in a 0.3% agar/media solution on top of the base layer at a concentration of 15,000 cells/well. Cells were fed with growth media on the first and sixth day after plating, stained with MTT, and imaged once colonies were visible. Colonies were counted using Image Quant (GE Healthcare).

Annexin V/PI Staining

Apoptosis was measured using the Annexin V: FITC Apoptosis Detection Kit per the manufacturer's protocol (BD Pharmingen, San Jose, CA, USA).

shRNA and CRISPR Studies

Lentivirus was generated by transfecting 293T cells with the appropriate lentiCRISPRv2 sgRNA vector or the appropriate pLKO shRNA vector, and the packaging plasmids pCMV8.9 and pCMV-VSVG, using Fugene 6 per the manufacturer's instructions (Promega). Forty-eight hrs after transfection, media containing virus was filtered through a 0.45 μM filter. Ewing sarcoma cell lines were transduced in 10 cm plates with 3 ml virus, 3 ml of growth media and 8 μg/ml polybrene (Sigma-Aldrich). Forty-eight hrs post-infection, cells were selected in puromycin–containing media. Five days post-selection (CRISPR studies) or three days post-selection (shRNA studies), cells were harvested for protein, colony formation and viability assays. CRISPR guide sequences were designed using the Broad Institute's sgRNA designer tool (http://www.broadinstitute.org/rnai/public/analysis-tools/sgrna-design-v1).

EWS/FLI knockdown was achieved using a TRIPZ inducible lentiviral vector system. Cells with either an shRNA against EWS/FLI or non-targeting control were treated with doxycycline every 48 hr for seven days. EWS/FLI knockdown was confirmed by western blotting. See Supplemental Table S6 for a list of all shRNA and sgRNA sequences and vector information.

Cell Viability and Synergy Studies

Cells were seeded onto 384-well tissue culture treated plates at a density of 25,000 cells/ml. After treatment with a compound or a combination of compounds, cells were analyzed for cell viability on days zero, three, five, and seven, using the Cell-TiterGlo luminescent assay (Promega) per the manufacturer's instructions. Luminescence was read on a Fluostar Omega Reader (BMG Labtech).

Chou-Talalay Combination Index for Loewe Additivity

Loewe additivity is a dose-effect model which states that additivity occurs in a two-drug combination if the sum of the ratios of the dose vs. the median-effect for each individual drug is 1. In this model, *combination index* (CI) scores estimate the interaction between the two drugs. If CI < 1, the drugs have a synergistic effect and if CI > 1, the drugs have an antagonistic effect. CI = 1 means the drugs have additive effect. Chou and Talalay (Chou and Talalay, 1984) showed that Loewe equations are valid for enzyme inhibitors with similar mechanisms of action -- either competitive or non-competitive toward the substrate. The combination index (*CI*) coefficients were computed based on the Chou-Talalay Median Effect model as implemented in *CalcuSyn* v2.11 (http://www.biosoft.com/w/calcusyn.htm). The degree of interaction between drugs was estimated according to the classification presented by Chou-Talalay (Chou and Talalay, 1984). The CI scores were computed for the range of concentrations of drug combinations where the effect of an individual drug was less than a fractional inhibition of 0.9. If the fractional inhibition score in paired combination with DMSO and with the other drug is > 0.9, this dose was eliminated from the analysis since the additional effect of the second drug could not be reliably calculated.

The Bliss Independence Method

Bliss independence (Bliss, 1956) is an effect-based strategy that compares the effect resulting from the combination of two drugs directly to the effects of its individual components.

The model predicts that if the individual drugs have the inhibitory effects f_1 and f_2 then the expected combined effect of the two drugs is:

$$E(f_{12}) = 1 - (1 - f_1)(1 - f_2) = f_1 + f_2 - f_1 f_2$$

The difference between the observed combined effect f_{12} and the *expected* combined effect of the two drugs is called the Excess over Bliss (eob): eob = $f_{12} - E(f_{12})$

Positive eob values are indicative of a synergistic interaction, whereas negative eob values are indicative of antagonistic behavior. Null *eob* values indicate no drug interaction.

Quantification and Statistical Analyses

GSEA v2.1.0, GraphPad PRISM 7, R 3.2.3 and Python 2.7.2 software packages were used to perform the statistical analyses. Statistical tests used are specified in the Figure legends. Errors bars represent standard deviation, unless otherwise stated. The threshold for statistical significance is $P < 0.05$, unless otherwise specified.

Data and Software Availability

Gene expression data have been deposited to GEO (accession no: GSE82270).

It can be accessed at: https://www.ncbi.nlm.nih.gov/geo/query/acc.cgi?acc=GSE82270

Supplementary Material

Refer to Web version on PubMed Central for supplementary material.

Acknowledgments

References

Bajrami I, Frankum JR, Konde A, Miller RE, Rehman FL, Brough R, Campbell J, Sims D, Rafiq R, Hooper S, et al. Genome-wide profiling of genetic synthetic lethality identifies CDK12 as a novel determinant of PARP1/2 inhibitor sensitivity. Cancer research. 2014; 74:287–297. [PubMed: 24240700]

Blazek D, Kohoutek J, Bartholomeeusen K, Johansen E, Hulinkova P, Luo Z, Cimermancic P, Ule J, Peterlin BM. The Cyclin K/Cdk12 complex maintains genomic stability via regulation of expression of DNA damage response genes. Genes & development. 2011; 25:2158–2172. [PubMed: 22012619]

Bliss CI. The calculation of microbial assays. Bacteriological reviews. 1956; 20:243–258. [PubMed: 13403845]

Brenner JC, Feng FY, Han S, Patel S, Goyal SV, Bou-Maroun LM, Liu M, Lonigro R, Prensner JR, Tomlins SA, Chinnaiyan AM. PARP-1 inhibition as a targeted strategy to treat Ewing's sarcoma. Cancer research. 2012; 72:1608–1613. [PubMed: 22287547]

Brohl AS, Solomon DA, Chang W, Wang J, Song Y, Sindiri S, Patidar R, Hurd L, Chen L, Shern JF, et al. The genomic landscape of the Ewing Sarcoma family of tumors reveals recurrent STAG2 mutation. PLoS genetics. 2014; 10:e1004475. [PubMed: 25010205]

Chipumuro E, Marco E, Christensen CL, Kwiatkowski N, Zhang T, Hatheway CM, Abraham BJ, Sharma B, Yeung C, Altabef A, et al. CDK7 inhibition suppresses super-enhancer-linked oncogenic transcription in MYCN-driven cancer. Cell. 2014; 159:1126–1139. [PubMed: 25416950]

Chou TC. Theoretical basis, experimental design, and computerized simulation of synergism and antagonism in drug combination studies. Pharmacological reviews. 2006; 58:621–681. [PubMed: 16968952]

Chou TC, Talalay P. Quantitative analysis of dose-effect relationships: the combined effects of multiple drugs or enzyme inhibitors. Advances in enzyme regulation. 1984; 22:27–55. [PubMed: 6382953]

Choy E, Butrynski JE, Harmon DC, Morgan JA, George S, Wagner AJ, D'Adamo D, Cote GM, Flamand Y, Benes CH, et al. Phase II study of olaparib in patients with refractory Ewing sarcoma following failure of standard chemotherapy. BMC cancer. 2014; 14:813. [PubMed: 25374341]

Christensen CL, Kwiatkowski N, Abraham BJ, Carretero J, Al-Shahrour F, Zhang T, Chipumuro E, Herter-Sprie GS, Akbay EA, Altabef A, et al. Targeting transcriptional addictions in small cell lung cancer with a covalent CDK7 inhibitor. Cancer cell. 2014; 26:909–922. [PubMed: 25490451]

Crompton BD, Stewart C, Taylor-Weiner A, Alexe G, Kurek KC, Calicchio ML, Kiezun A, Carter SL, Shukla SA, Mehta SS, et al. The Genomic Landscape of Pediatric Ewing Sarcoma. Cancer discovery. 2014

Ekumi KM, Paculova H, Lenasi T, Pospichalova V, Bosken CA, Rybarikova J, Bryja V, Geyer M, Blazek D, Barboric M. Ovarian carcinoma CDK12 mutations misregulate expression of DNA

repair genes via deficient formation and function of the Cdk12/CycK complex. Nucleic acids research. 2015; 43:2575–2589. [PubMed: 25712099]

Garnett MJ, Edelman EJ, Heidorn SJ, Greenman CD, Dastur A, Lau KW, Greninger P, Thompson IR, Luo X, Soares J, et al. Systematic identification of genomic markers of drug sensitivity in cancer cells. Nature. 2012; 483:570–575. [PubMed: 22460902]

Gill SJ, Travers J, Pshenichnaya I, Kogera FA, Barthorpe S, Mironenko T, Richardson L, Benes CH, Stratton MR, McDermott U, et al. Combinations of PARP Inhibitors with Temozolomide Drive PARP1 Trapping and Apoptosis in Ewing's Sarcoma. PloS one. 2015; 10:e0140988. [PubMed: 26505995]

Greco WR, Bravo G, Parsons JC. The search for synergy: a critical review from a response surface perspective. Pharmacological reviews. 1995; 47:331–385. [PubMed: 7568331]

Hu-Lieskovan S, Heidel JD, Bartlett DW, Davis ME, Triche TJ. Sequence-specific knockdown of EWS-FLI1 by targeted, nonviral delivery of small interfering RNA inhibits tumor growth in a murine model of metastatic Ewing's sarcoma. Cancer research. 2005; 65:8984–8992. [PubMed: 16204072]

Johnson SF, Cruz C, Greifenberg AK, Dust S, Stover DG, Chi D, Primack B, Cao S, Bernhardy AJ, Coulson R, et al. CDK12 Inhibition Reverses De Novo and Acquired PARP Inhibitor Resistance in BRCA Wild-Type and Mutated Models of Triple-Negative Breast Cancer. Cell reports. 2016; 17:2367–2381. [PubMed: 27880910]

Joshi PM, Sutor SL, Huntoon CJ, Karnitz LM. Ovarian cancer-associated mutations disable catalytic activity of CDK12, a kinase that promotes homologous recombination repair and resistance to cisplatin and poly(ADP-ribose) polymerase inhibitors. The Journal of biological chemistry. 2014; 289:9247–9253. [PubMed: 24554720]

Kaelin WG Jr. The concept of synthetic lethality in the context of anticancer therapy. Nature reviews Cancer. 2005; 5:689–698. [PubMed: 16110319]

Kennedy AL, Vallurupalli M, Chen L, Crompton B, Cowley G, Vazquez F, Weir BA, Tsherniak A, Parasuraman S, Kim S, et al. Functional, chemical genomic, and super-enhancer screening identify sensitivity to cyclin D1/CDK4 pathway inhibition in Ewing sarcoma. Oncotarget. 2015; 6:30178–30193. [PubMed: 26337082]

Kwiatkowski N, Zhang T, Rahl PB, Abraham BJ, Reddy J, Ficarro SB, Dastur A, Amzallag A, Ramaswamy S, Tesar B, et al. Targeting transcription regulation in cancer with a covalent CDK7 inhibitor. Nature. 2014; 511:616–620. [PubMed: 25043025]

Lawrence MS, Stojanov P, Polak P, Kryukov GV, Cibulskis K, Sivachenko A, Carter SL, Stewart C, Mermel CH, Roberts SA, et al. Mutational heterogeneity in cancer and the search for new cancer associated genes. Nature. 2013; 499:214–218. [PubMed: 23770567]

Liang K, Gao X, Gilmore JM, Florens L, Washburn MP, Smith E, Shilatifard A. Characterization of human cyclin-dependent kinase 12 (CDK12) and CDK13 complexes in C-terminal domain phosphorylation, gene transcription, and RNA processing. Molecular and cellular biology. 2015; 35:928–938. [PubMed: 25561469]

Loven J, Orlando DA, Sigova AA, Lin CY, Rahl PB, Burge CB, Levens DL, Lee TI, Young RA. Revisiting global gene expression analysis. Cell. 2012; 151:476–482. [PubMed: 23101621]

Marques Howarth M, Simpson D, Ngok SP, Nieves B, Chen R, Siprashvili Z, Vaka D, Breese MR, Crompton BD, Alexe G, et al. Long noncoding RNA EWSAT1-mediated gene repression facilitates Ewing sarcoma oncogenesis. The Journal of clinical investigation. 2014; 124:5275–5290. [PubMed: 25401475]

Meyers RM, Bryan JG, McFarland JM, Weir BA, Sizemore AE, Xu H, Dharia NV, Montgomery PG, Cowley GS, Pantel S, et al. Computational correction of copy-number effect improves specificity of CRISPR-Cas9 essentiality screens in cancer cells. Nature Genetics. 2017 In Press.

Monterrubio C, Paco S, Vila-Ubach M, Rodriguez E, Glisoni R, Lavarino C, Schaiquevich P, Sosnik A, Mora J, Carcaboso AM. Combined Microdialysis-Tumor Homogenate Method for the Study of the Steady State Compartmental Distribution of a Hydrophobic Anticancer Drug in Patient-Derived Xenografts. Pharmaceutical research. 2015; 32:2889–2900. [PubMed: 25773723]

Nieto-Soler M, Morgado-Palacin I, Lafarga V, Lecona E, Murga M, Callen E, Azorin D, Alonso J, LopezContreras AJ, Nussenzweig A, Fernandez-Capetillo O. Efficacy of ATR inhibitors as single agents in Ewing sarcoma. Oncotarget. 2016; 7:58759–58767. [PubMed: 27577084]

Norris RE, Adamson PC, Nguyen VT, Fox E. Preclinical evaluation of the PARP inhibitor, olaparib, in combination with cytotoxic chemotherapy in pediatric solid tumors. Pediatric blood & cancer. 2014; 61:145150.

Ordonez JL, Amaral AT, Carcaboso AM, Herrero-Martin D, del Carmen Garcia-Macias M, Sevillano V, Alonso D, Pascual-Pasto G, San-Segundo L, Vila-Ubach M, et al. The PARP inhibitor olaparib enhances the sensitivity of Ewing sarcoma to trabectedin. Oncotarget. 2015; 6:18875–18890. [PubMed: 26056084]

Riggi N, Knoechel B, Gillespie SM, Rheinbay E, Boulay G, Suva ML, Rossetti NE, Boonseng WE, Oksuz O, Cook EB, et al. EWS-FLI1 utilizes divergent chromatin remodeling mechanisms to directly activate or repress enhancer elements in Ewing sarcoma. Cancer cell. 2014; 26:668–681. [PubMed: 25453903]

Sanjana NE, Shalem O, Zhang F. Improved vectors and genome-wide libraries for CRISPR screening. Nature methods. 2014; 11:783–784. [PubMed: 25075903]

Smith R, Owen LA, Trem DJ, Wong JS, Whangbo JS, Golub TR, Lessnick SL. Expression profiling of EWS/FLI identifies NKX2.2 as a critical target gene in Ewing's sarcoma. Cancer cell. 2006; 9:405–416. [PubMed: 16697960]

Sonnenblick A, de Azambuja E, Azim HA Jr, Piccart M. An update on PARP inhibitors--moving to the adjuvant setting. Nature reviews Clinical oncology. 2015; 12:27–41.

Stewart E, Goshorn R, Bradley C, Griffiths LM, Benavente C, Twarog NR, Miller GM, Caufield W, Freeman BB 3rd, Bahrami A, et al. Targeting the DNA repair pathway in Ewing sarcoma. Cell reports. 2014; 9:829–841. [PubMed: 25437539]

Tirode F, Surdez D, Ma X, Parker M, Le Deley MC, Bahrami A, Zhang Z, Lapouble E, GrosseteteLalami S, Rusch M, et al. Genomic landscape of Ewing sarcoma defines an aggressive subtype with co-association of STAG2 and TP53 mutations. Cancer discovery. 2014; 4:1342–1353. [PubMed: 25223734]

Tomazou EM, Sheffield NC, Schmidl C, Schuster M, Schonegger A, Datlinger P, Kubicek S, Bock C, Kovar H. Epigenome mapping reveals distinct modes of gene regulation and widespread enhancer reprogramming by the oncogenic fusion protein EWS-FLI1. Cell reports. 2015; 10:1082–1095. [PubMed: 25704812]

Vormoor B, Curtin NJ. Poly(ADP-ribose) polymerase inhibitors in Ewing sarcoma. Current opinion in oncology. 2014; 26:428–433. [PubMed: 24840521]

Yang W, Soares J, Greninger P, Edelman EJ, Lightfoot H, Forbes S, Bindal N, Beare D, Smith JA, Thompson IR, et al. Genomics of Drug Sensitivity in Cancer (GDSC): a resource for therapeutic biomarker discovery in cancer cells. Nucleic acids research. 2013; 41:D955–961. [PubMed: 23180760]

Zhang T, Kwiatkowski N, Olson CM, Dixon-Clarke SE, Abraham BJ, Greifenberg AK, Ficarro SB, Elkins JM, Liang Y, Hannett NM, et al. Covalent targeting of remote cysteine residues to develop CDK12 and CDK13 inhibitors. Nature chemical biology. 2016; 12:876–884. [PubMed: 27571479]

SIGNIFICANCE

Here we report that Ewing sarcoma is a disease with exquisite sensitivity to the covalent small molecule CDK7/12/13 inhibitors, THZ1 and THZ531. These compounds act, in part, through inhibition of CDK12 and the subsequent suppression of genes involved in DNA damage repair. The preferential sensitivity of Ewing sarcoma cells to THZ1/THZ531 is imparted by the tumor-specific expression of the fusion oncoprotein EWS/FLI. The combination of these molecules with PARP inhibitors showed prominent synergy in multiple models of Ewing sarcoma without apparent toxicity. With this class of compounds moving toward the clinic, this study has promising translational potential for patients with Ewing sarcoma and important translational relevance to other tumors that are sensitive to PARP inhibitors.

HIGHLIGHTS

1. Ewing sarcoma cells are highly sensitive to CDK7/12/13 inhibitors.

2. Tumor-specific EWS/FLI expression is synthetic lethal with suppression of CDK12.

3. CDK12/13 inhibitors impair DNA damage repair in fusion-positive Ewing sarcoma.

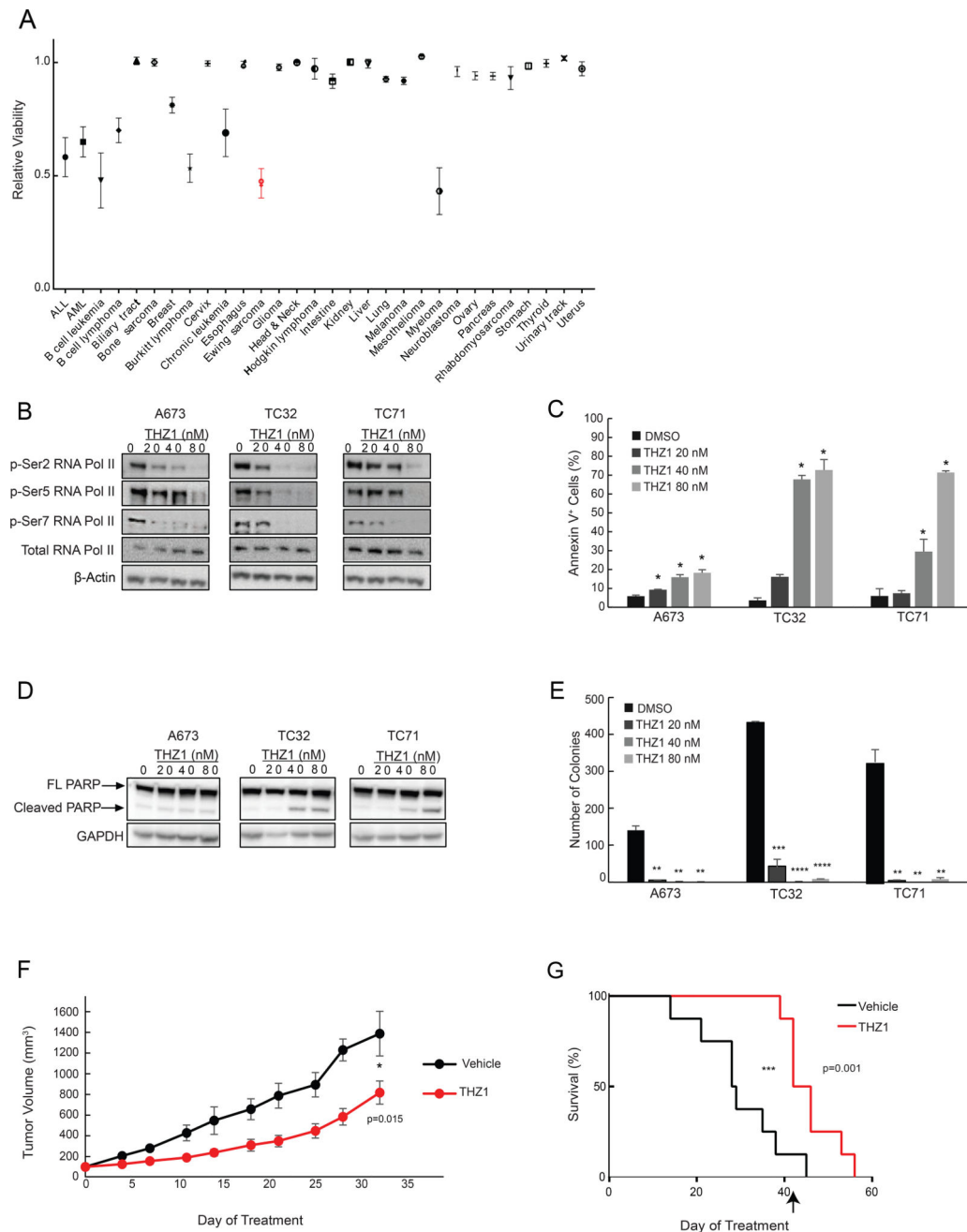4. CDK12/13 and PARP inhibitors are highly synergistic in Ewing sarcoma.

Figure 1. Extensive profiling of THZ1 highlights exceptional sensitivity of Ewing sarcoma cells
A. A diverse panel of 1,081 cancer cell lines was treated with DMSO or 9.76 nM THZ1 for 72 hr and assayed for cell viability. Shown are the mean relative viabilities +/− SEM for each tumor type with at least eight cell lines screened. Ewing sarcoma cell lines are in red. **B.** Western blot demonstrating the effects of THZ1 on p-RNA Pol II in Ewing sarcoma cell lines at 6 hr. β-Actin, loading control. **C.** Concentration-dependent effects of THZ1 on the percentage of Annexin V^+ cells measured by flow cytometry at 24 hr. Data are presented as mean values ± SD of triplicate points (t-test). **D.** Western blot demonstrating the effects of THZ1 on PARP cleavage at 24 hr. GAPDH, loading control. **E.** Colony formation in soft

agar of Ewing sarcoma cell lines treated with THZ1 for 14 days. The experiment was conducted in biological triplicate. Data shown is a representative experiment of mean values ± SD of technical duplicates (t-test). **F.** Tumor volume measurements of TC32 Ewing sarcoma xenografts treated with 10 mg/kg THZ1 IP or vehicle control (10% DMSO in D5W) IP BID. Data are plotted out to day 32 when >50% of mice in the vehicle group were still alive and presented as mean values ± SD (n=8 per arm) (t-test). **G.** Kaplan Meier survival curves for the experiment described in **F.** Treatment was stopped on day 42 (arrow) and mice were followed for survival (Log-rank Mantel Cox test). *p value <0.05, **p value <0.01, ***p value <0.001, ****p value <0.0001. See also Figure S1.
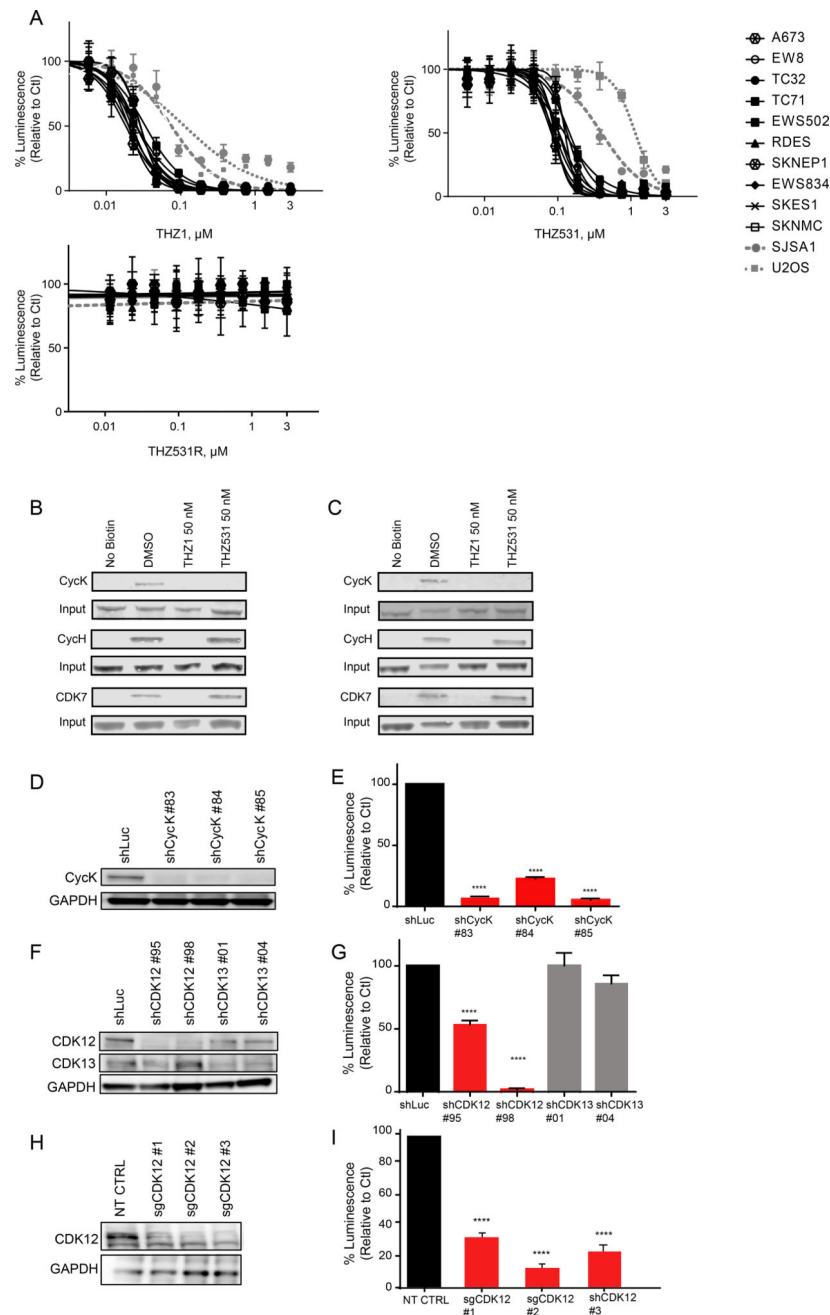
Figure 2. The activity of THZ1 in Ewing sarcoma cell lines is attributed to CDK12 inhibition
A. Dose-response curves of Ewing sarcoma cell lines (black) and osteosarcoma cell lines (gray) treated with THZ1 (CDK7/12/13 inhibitor), THZ531 (CDK12/13 selective inhibitor), or THZ531R (derivative of THZ531 that lacks the covalent binding moiety) for 72 hr. Data are plotted as the percentage of luminescence relative to DMSO controls. The experiment was performed in biological triplicate. Results are presented as mean values of a representative experiment ± SD of 8 technical replicates. **B–C.** THZ1-biotin immunoprecipitation of samples treated with THZ1 or THZ531 and probed for Cyclin K (CycK) or Cyclin H (CycH) in A673 cells **(B)** and TC32 cells **(C)**. The experiment was

performed in biological duplicate. **D.** Immunoblot of A673 cells infected with a luciferase shRNA control (shLuc) or shRNAs against Cyclin K (shCycK) and probed for Cyclin K expression five days post-infection. GAPDH, loading control. **E.** Relative viability of A673 cells infected with shLuc or shCycK ten days post-infection. Data are plotted as the percentage of luminescence relative to shLuc control. The experiment was performed in biological triplicate. Results are presented as mean values of a representative experiment ± SD of 8 technical replicates. (Statistical significance is calculated for each individual hairpin compared to the control hairpin, t-test). **F.** Immunoblot of A673 cells infected with a luciferase shRNA control or shRNAs against CDK12 or CDK13 five days post-infection. GAPDH, loading control. **G.** Relative viability of cells infected with hairpins against luciferase, CDK12 or CDK13 ten days post-infection. Data are plotted as the percentage of luminescence relative to shLuc control. The experiment was performed in biological triplicate. Results are presented as mean values of a representative experiment ± SD of 8 technical replicate. (Statistical significance is calculated for each individual hairpin compared to the control hairpin, t-test). **H.** Immunoblot of A673 cells infected with a non-targeting control sgRNA (NT CTRL) or three different guide RNAs against *CDK12* (sgCDK12) seven days post-infection. GAPDH, loading control. **I.** Relative viability of cells infected with a NT CTRL sgRNA or sgRNAs targeting *CDK12* fourteen days post-infection. Data are plotted as the percentage of luminescence relative to NT control. The experiment was performed in biological triplicate. Results are presented as mean values of a representative experiment ± SD of 8 technical replicates. (Statistical significance is calculated for each individual hairpin compared to the control hairpin, t-test). ****p value <0.0001. See also Figure S2 and Tables S1 and S2.
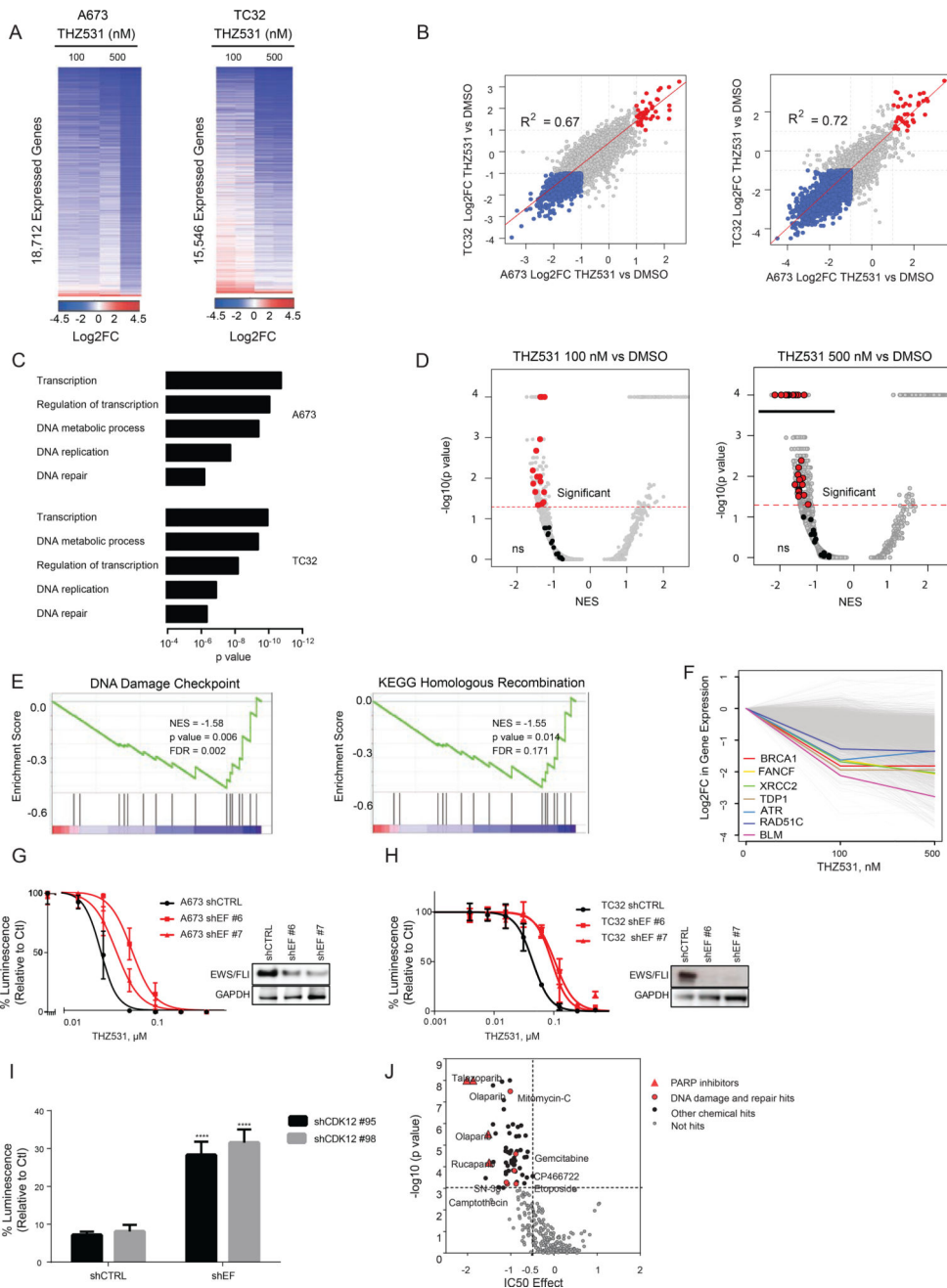
Figure 3. THZ531 treatment globally downregulates mRNA levels with enrichment for suppression of DNA damage/repair-related genes

A. A673 and TC32 cells were treated with THZ531 for 6 hr in duplicate. Heatmaps display the log2 fold change (Log2FC) in gene expression for THZ531 vs. DMSO treatment. **B.** Log2FCs in gene expression in A673 cells (x-axis) or TC32 cells (y-axis) treated with 100 nM THZ531 vs. DMSO (left) or 500 nM THZ531 vs. DMSO (right). Genes are represented as dots. Dots corresponding to genes significantly downregulated by THZ531 in both A673 and TC32 lines are highlighted blue. Dots corresponding to genes significantly upregulated by THZ531 in both A673 and TC32 cells are highlighted red. The Log2FCs in gene expression in A673 cells vs. TC32 cells are positively correlated with 100 nM THZ531 (R^2

= 0.67) and 500 nM THZ531 (R^2 = 0.72). **C.** Gene Ontology analysis of the top 5% of sensitive genes to 100 nM THZ531 treatment. **D.** Volcano plot depicting GSEA for enrichment from the MSigDB v5 collections, c2, and c5, as well as published EWS/FLI genes sets, in the genes significantly downregulated by 100 nM THZ531 in both A673 and TC32 cells. DNA damage response (DDR) gene sets are highlighted in red and EWS/FLI1 gene sets are highlighted in black. Gene sets that fall above the red line are statistically significant. Positive normalized enrichment scores (NES) indicate upregulation of genes sets, whereas, negative NES indicate downregulation of gene sets. ns = not significant. **E.** Individual GSEA plots for enrichment of the indicated gene sets among THZ531 downregulated genes. **F.** Graph showing the Log2FC in gene expression after 100 nM and 500 nM THZ531 treatment with select DDR genes highlighted. **G–H.** Dose-response curves of A673 shCTRL and shEWS/FLI **(G)** and TC32 shCTRL and shEWS/FLI cells **(H)** generated with two distinct hairpins treated with THZ531 for 72 hr. Data are plotted as the percentage of luminescence relative to DMSO controls. Experiments were conducted in biological triplicate. Results are presented as mean values of a representative experiment ± SD of 8 technical replicates. Western blots demonstrating EWS/FLI knockdown are shown to the right of the dose response curves. **I.** Relative viability of A673 shCTRL and shEWS/FLI cells infected with hairpins against CDK12 seven days post-infection. Data are plotted as the percentage of luminescence relative to shCTRL cells. The experiment was conducted in biological triplicate. Results are presented as mean values of a representative experiment ± SD of 8 technical replicates. (Statistical significance is calculated for the viability effect of each CDK12 hairpin in the context of shEWS/FLI compared to shCTRL, ****p value <0.0001, t-test). **J.** EWS/FLI biomarker data from the Genomics of Drug Sensitivity in Cancer (http://cancerrxgene.org, release 21-41-36, June 2 2017). Enrichment of drugs targeting DDR Pathways among drugs in which EWS/FLI is a biomarker of sensitivity was calculated by Two-tailed Fisher exact test: Odds Ratios = 3.81, p value = 0.0078. Significant hits cut-offs: IC_{50} Effect < −0.5, p value < 0.001. PARP inhibitors are shown as red triangles, additional DNA damage and repair drugs as red circles, and other chemical hits as black circles. Olaparib was screened at 5 and 10 nM. See also Figures S3 and Tables S3–S5.
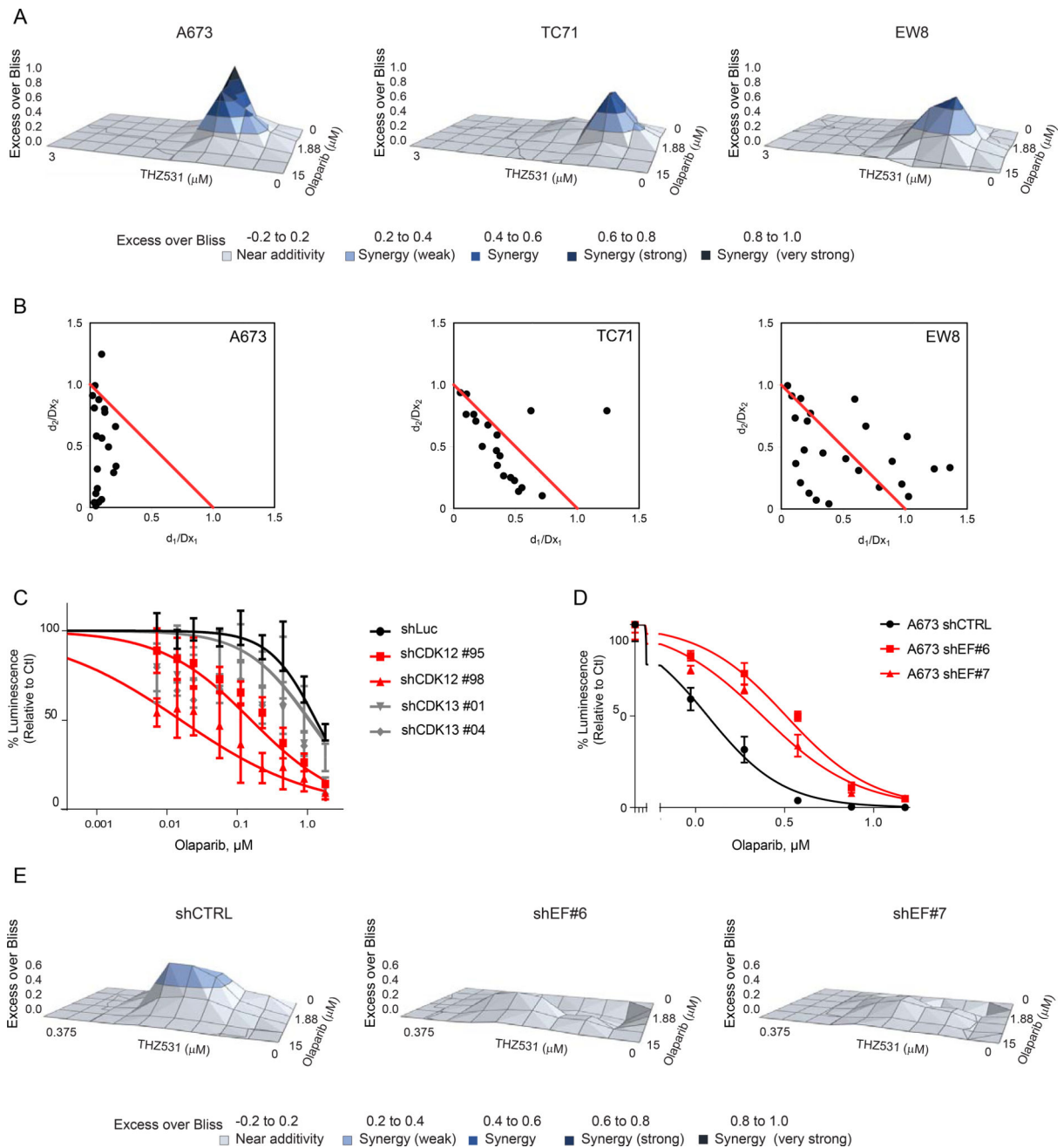
Figure 4. THZ531 synergy with olaparib is EWS/FLI dependent

A. Excess over Bliss synergy plots for serial dilutions of THZ531 in combination with olaparib in A673, TC71 and EW8 cells. Excess over Bliss scores > 0 indicate drug synergy, whereas negative scores indicate antagonism. **B.** Chou-Talalay normalized isobolograms of data presented in **(A)**. Plots depict combination index scores over a range of concentrations of THZ531 and olaparib. The coordinates of the CI scores are d_1/D_{x1} and d_2/D_{x2} where D_{x1} is the concentration of drug 1 (THZ531) that alone produces the fractional inhibition effect x, and D_{x2} is the concentration of drug 2 (olaparib) that alone produces the fractional inhibition effect x. CI < 1 = synergism, CI > 1 = antagonism. The red line displayed is the

line of additivity. **C.** Dose-response curves of A673 cells infected with hairpins against luciferase, CDK12, or CDK13, and treated with olaparib for five days. Data are plotted as the percentage of luminescence relative to shLuc control. The experiment was conducted in biological duplicate. Results are presented as mean values of a representative experiment ± SD of 8 technical replicates. **D.** Dose-response curves of A673 shCTRL and shEWS/FLI cells treated with olaparib for five days. Data are plotted as the percentage of luminescence relative to DMSO controls. The experiment was conducted in biological triplicate. Results are presented as mean values of a representative experiment ± SD of 8 technical replicates. **E.** THZ531 and olaparib excess over Bliss synergy plots in A673 shCTRL and shEWS/FLI cells. The experiment was conducted in biological triplicate. See also Figure S4.
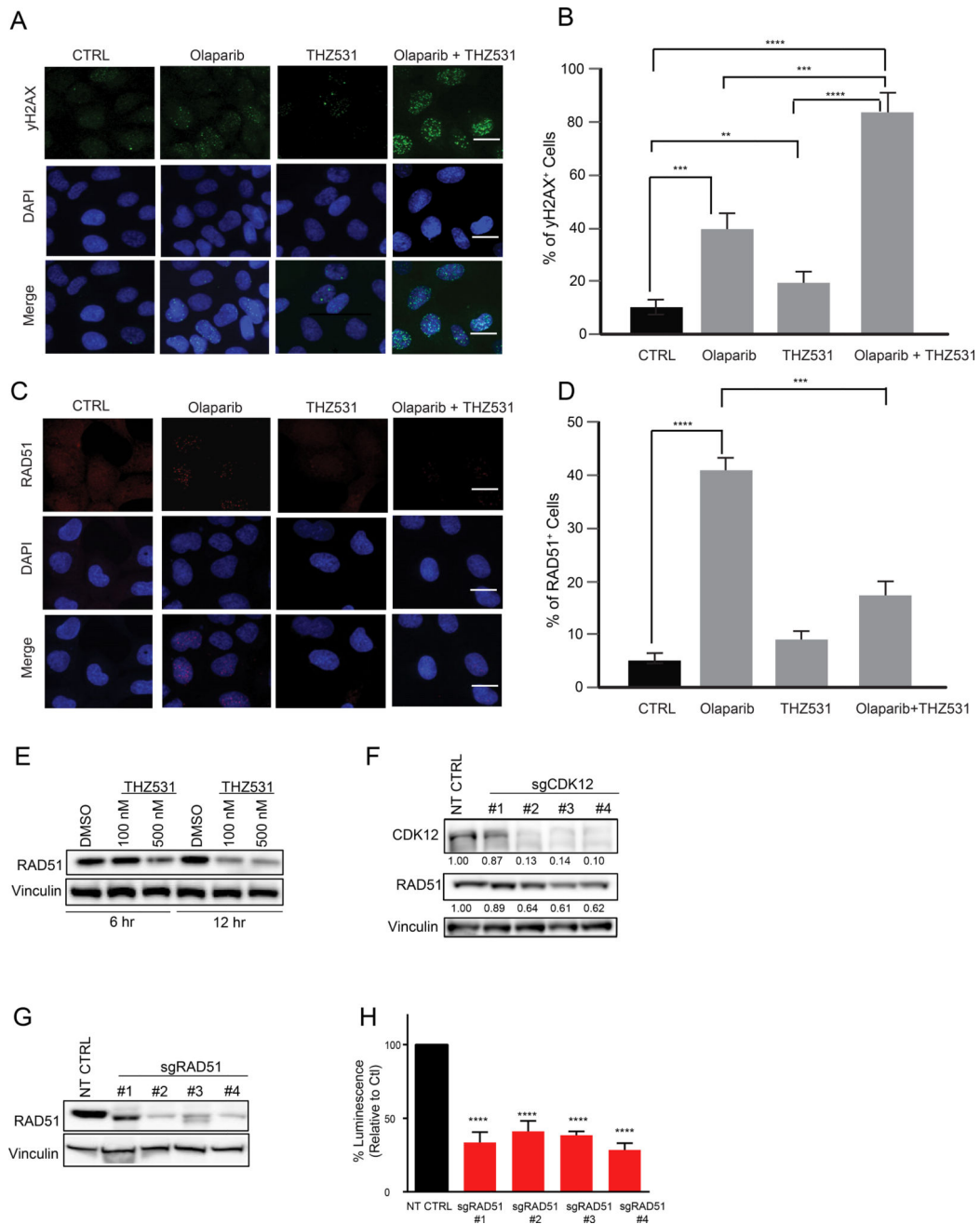
Figure 5. THZ531 and olaparib synergistically induce DNA damage in Ewing sarcoma cells

A–D. γH2AX foci staining (**A**) and quantification (**B**), and Rad51 foci staining (**C**) and quantification (**D**) in A673 cells treated with olaparib (2 μM) or THZ531 (25 nM) alone and in combination for 72 hr. Nuclei are stained with DAPI. Scale bars represent 5 μM. One hundred cells per sample were counted and results are presented as mean values ± SD (t-test). A cell was counted as positive if >10 foci per nucleus were identified. **E.** Immunoblot of A673 cell lysates treated with DMSO or THZ531 and probed for RAD51 expression. Vinculin, loading control. **F.** Immunoblot of A673 cells infected with a NT CTRL or guide RNAs targeting *CDK12* and probed for CDK12 and RAD51. Vinculin, loading control.

Densitometric quantification is shown below the blots for CDK12 and RAD51. Values are normalized to the vinculin expression for each condition and then to the expression in the NT CTRL. **G.** Immunoblot of A673 cells infected with a NT CTRL or guide RNAs targeting *RAD51* seven days post-infection. Vinculin, loading control. **H.** Viability of cells infected with sgRNAs against *RAD51* 14 days post-infection. Data are plotted as the percentage of luminescence relative to NT CTRL. The experiment was conducted in biological triplicate. Results are presented as mean values of a representative experiment ± SD of 8 technical replicates (t-test). **p value <0.01, ***p value <0.001, ****p value <0.0001.
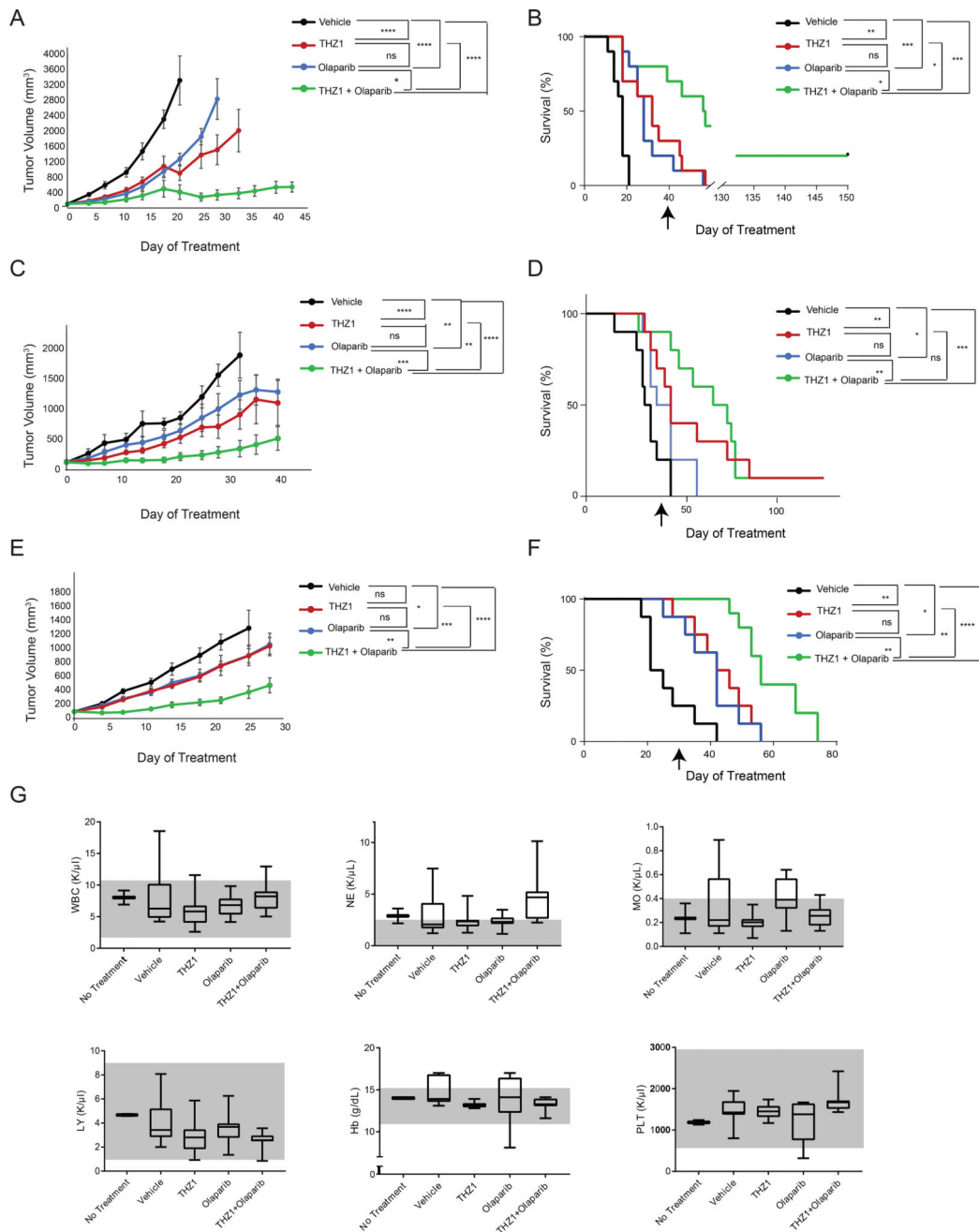
Figure 6. THZ1 and olaparib are strongly synergistic in several mouse models of Ewing sarcoma
A. Tumor volume measurements of an A673 xenograft mouse model treated with vehicle, 10 mg/kg THZ1 IP BID, 50 mg/kg olaparib PO BID, or the combination of olaparib+THZ1. Treatment was stopped on day 40. Data for a given time point were plotted if >50% of mice in the group were alive. Data are plotted as mean values ± SD (n=10 per arm). **B**. Kaplan Meier survival curves for the experiment described in **(A).** Arrow indicates treatment end date. **C.** Tumor volume measurements of a TC71 xenograft mouse model treated with vehicle, 10 mg/kg THZ1 IP BID, 50 mg/kg olaparib PO BID, or the combination of olaparib +THZ1. Treatment was stopped on day 40. Data for a given time point were plotted if >50%

of mice in the group were alive. Data are plotted as mean values ± SD (n=10 per arm). **D.** Kaplan Meier survival curves for the experiment described in **(C).** Arrow indicates treatment end date. **E.** Tumor volume measurements of a PDX mouse model of Ewing sarcoma treated with vehicle, 10 mg/kg THZ1 IP BID, 50 mg/kg olaparib PO BID, or the combination of olaparib+THZ1. Treatment was stopped on day 28. Data for a given time point were plotted if >50% of mice in the group were alive. Data are plotted as mean values ± SD (n=8 per arm). **F.** Kaplan Meier survival curves for the experiment described in **(E).** Arrow indicates treatment end date. (ns = not significant, *p value <0.05, **p value <0.01, ***p value <0.001. ****p value <0.0001. 2 way ANOVA with Tukey *post hoc* test was performed for tumor volume graphs and Log-rank Mantel Cox test was performed for survival curves. **G.** Complete blood count analysis of TC71 xenografted mice treated as in **(C)** at time of sacrifice. Mice were sacrificed when tumors reached 2 cm in length, and in some cases, mice were off treatment at time of sacrifice. Two mice that were never on treatment were included as additional controls. The gray areas mark the normal range for each blood cell count and are measured in thousands per cubic milliliter (K/μL) of blood. WBC = white blood cells, NE = neutrophils, MO = monocytes, LY = lymphocytes, Hb = hemoglobin, PLT = platelets. Data are presented as mean values with whiskers representing min and max values and the outer edges of the boxes representing the 25th percentile (lower quartile) and 75th percentile (upper quartile). ns = not significant, *p value <0.05, **p value <0.01, ***p value <0.001, ****p value <0.0001. See also Figures S5.